ARP@VST: legacy survey of the Arp peculiar galaxies with the VST

Abstract

The VLT Survey Telescope (VST) is a 2.6-m optical wide-field telescope installed at the ESO observatory of Cerro Paranal (Chile). The only instrument at the VST is OmegaCAM, which is a wide-field camera, covering 1 square degree in the sky, with 0.21 arcsec per pixel. On 1st October 2022, after more than 10 years of activity, the INAF-ESO contract expired and the VST became a hosted telescope at ESO. VST is currently owned and managed by INAF, and a new 5-year, 2022-2027 (renewable) INAF-ESO agreement was signed to define rules and roles.
Since then, the INAF-Coordination Centre for the VST is in charge of managing the operations at the VST.
The VST is the ideal instrument for mapping the outskirts of galaxies in depth, down to the low surface brightness levels necessary to reveal weak structures such as tidal tails, satellites, and halos, signs of past gravitational interactions and galactic mergers. For this reason, the INAF-Coordination Centre for the VST decided to revisit the Arp's catalog by creating a public survey dedicated to the peculiar Arp galaxies visible from the southern hemisphere.
Arp@VST is a multi-band imaging survey of the peculiar galaxies in the ARP catalog with VST, visible from the ESO Cerro-Paranal Observatory
This is a public observing program, where we commit to producing and making publicly available the fully reduced data set
Given the excellent capabilities of the VST to map the galaxies' outskirts, down to the low surface brightness levels needed to detect and study the remnants of the gravitational interactions and merging, with the present project we plan to acquire deep images in the g and r bands, down to $\mu g \sim 28 - 31$ mag/arcsec^2, for all the Arp galaxies visible from the Paranal Observatory (DEC < +10 deg), to detect the LSB features (in the form of stellar streams or tidal tails) out to unprecedented distances from the center of the target (~10 Re). Shallower images are requested in the i band and with Hα filter, which can be acquired in the bright time.
We plan to release new reduced data as soon as they are observed and processed.

Overview of Observations

The Atlas of Peculiar Galaxies was produced by Halton Arp in 1966. The catalog contains 338 galaxies with distorted morphologies and/or interacting systems, spanning an optical magnitude from 6 to 17 mag, with a peak around 13-14 mag. The Atlas images were acquired with the Hale and Schmidt telescopes of the Carnegie Observatories, providing the best photographic plates of the time, which revealed the faint galactic details with very high resolution.

As stated in the preface of Arp's catalog, "the peculiarities of the galaxies pictured in this Atlas represent perturbations, deformations, and interactions which should enable us to analyze the nature of the real galaxies which we observe and which are too remote to experiment on directly."

This sentence summarizes Arp's main goal for this catalog. At that time, the physical processes that shaped the Hubble sequence galaxies were not fully understood. Therefore, the Arp catalog aimed at providing examples of the different kinds of peculiar structures found in galaxies to be considered "laboratories" where astronomers can study the mechanisms acting on the main sequence galaxies, i.e. spiral or elliptical galaxies.

The atlas does not include all kinds of peculiar galaxies known to date. It collects several examples of gravitational interactions between galaxies, grouped as follows:

- individual peculiar spiral galaxies or spiral galaxies that apparently have small companions
- elliptical-like galaxies
- individual or groups of galaxies with distorted morphology
- double galaxies.

Some examples are shown in Fig.1 and Fig.2.

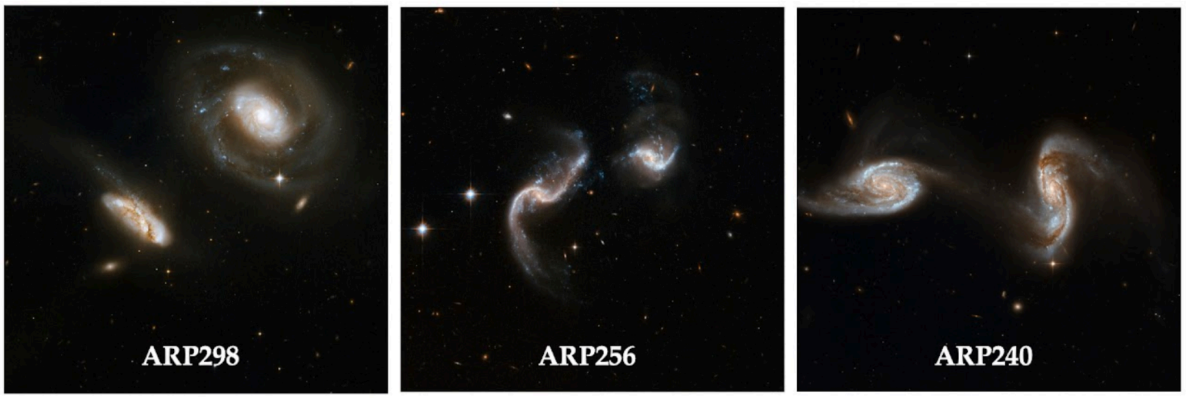

Figure 1: HST images of ARP galaxies, included in the target list of this collection. Here there are examples of interacting spiral galaxies with tidal tails and distorted morphologies.

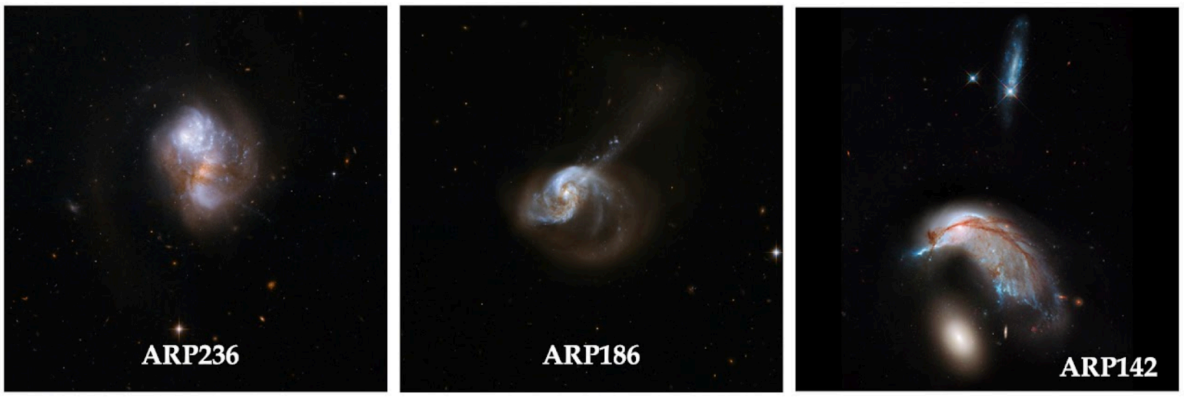

Figure 2: HST images of ARP galaxies, included in the target list of this collection. Here there are examples of final merger remnant, where the regular structure of the parent galaxies is completely lost.

The main science deliverables that this public survey can offer are the following:

- Interaction and merging: combining the deep images acquired in the g and r bands and the large covered area of the VST data proposed here, the tidal tails or stellar streams can be detected down to the faintest levels of μg∼28 − 31 mag/arcsec^2 and out to unexplored regions, at larger radii from the target centre. The structure of these features can be directly compared with the predictions of all phases of the gravitational merging between galaxies with different mass ratios.

The main outcome of these studies is to provide more stringent constraints on the formation of massive early-type galaxies and the mass assembly process.

- Detection of small satellites: to date, the confirmation of the LCDM cosmological model relies on our ability to find the baryonic counterparts of the predicted low-mass DM halos, which means deriving a complete census of the faintest, less massive stellar systems such as dwarf galaxies. In this context, the UDGs have a special role, being the extreme LSB tail of the size-luminosity distribution of dwarf galaxies. The depth and the large FOV of the acquired images can offer a unique opportunity to improve the detection of the satellites dwarfs galaxies, in particular the most low surface brightness and diffuse systems.
- Detection and formation of the tidal dwarfs and tidal UDGs: as a follow-up in the detection of the dwarf galaxies, cited above, this project provides an excellent sample of interacting galaxies, where a statistically significant sample of tidal-dwarf galaxies can be detected. These kinds of systems, formed in the tidal tails of the merging spiral galaxies, are particularly interesting since they are DM-free (Duc et al. 2015). The structure and stability of these galaxies are still an open issue to be investigated.
- Distribution of dust in the galaxy structure: the g-i color maps can be used to trace the regions of dust absorption inside each galaxy.
- Star formation regions: the Hα images acquired with this project can be used (i) to identify and study the star-forming regions and determine whether they might have been affected by environmental interactions: any asymmetry in the star formation rate map derived from Hα can indicate whether (and in which part) a galaxy is experiencing a star formation rate enhancement or a possible quenching of star formation; (ii) to identify displacement of ionized gas with respect to the stellar component, which might reveal on-going (and possibly subtle) hydrodynamical interactions. This offers the exquisite opportunity to identify interesting regions for further follow-ups to understand how gas is being removed.
- Spectral Energy Distribution: combining the multi-bands images released with this proposal, which cover the optical wavelength range, with available data in other bands, from UV to NIR, the spectral energy distribution can be addressed for each target of the sample. An example of such a kind of analysis, by combining the UV data with the optical VST images, Rampazzo et al. (2022) derived the star formation history of the galaxies in the Dorado group.
- Dissemination of knowledge: ARP galaxies are truly fascinating objects: with their curious shapes and intricate features, they do not only attract the attention of astronomers but may also trigger the curiosity of the general public. Therefore, the multi-band images obtained from this project can be used to produce spectacular color-composite images, to be widely distributed via the INAF online media channels. Astronomical images are widely featured by national and international media and tend to be extensively appreciated and shared on image-based social media platforms that are popular with the young public. In combination with existing Hubble space telescope images, which depict ARP galaxies and their immediate surroundings, VST images help paint a broader picture of the “lives” of galaxies, by showing tidal tails and other effects of their interactions on a much broader scale, thus providing a more complete story of galaxy evolution and demonstrating the complementarity of multiple telescopes with different characteristics. Once the program is completed, the collection of images can form the core of a coffee-table book showcasing beautiful views of the cosmos as observed by the VST.
- Finally, all targets in the catalog can be explored more in detail with follow-up studies, using different observing facilities and instruments.

Survey Plan

The use of VST for this project has two main reasons: the large field of view (FOV) and the high arcsec-level angular resolution of OmegaCam.
The large FOV is necessary to map the structure of the galaxies’ outskirts out to an unprecedented radius, more than 10 Re (see Figure 3).
A bunch (18) of the Arp galaxies have been observed with the HST. Although HST images have better angular resolution than ground-based VST images, the FOV of the HST is significantly smaller than 1 square degree. Specifically, Arp images taken with ACS/WFC have a FOV approximately 300 times smaller than that of the VST, while those taken with WFC3 and WFPC2 are about 500 times smaller. Therefore,

they provide a limited view of the faint features in the galaxies' outskirts of the Arp targets. With the large area covered with VST, we can extend the detection and analysis of these features.
The large FOV, combined with the resolution of 0.21 arcsec/pixels is fundamental to improving the detection of the satellite galaxies in the outskirts and to resolving the fine features in the tidal tails, like the star-forming clumps. Furthermore, VST mounts a narrow band Hα filter (NB_659) divided into 4 quadrants (see Drew et al. 2014), which are all centered at ~6590Å. Since our targets are all in the local Universe (z~0), it will allow us to take advantage of the full VST FoV while searching for Hα emission.
Data in the g and r bands are acquired in dark and grey time (FLI<0.3 - 0.5), respectively, under an average seeing $\leq$ 1.3 arcsec conditions. With the total integration times of 2.5 hrs in both bands, result in the measured surface brightness depth for a point source at 5 sigma, over an area of FWHM~1 arcsec, reaches μg=27.3 mag and μr=28.9 mag, respectively.
Given the larger collecting area with the galactocentric radius, the limiting surface brightness of the azimuthally averaged surface brightness profiles are deeper: μg~28−30 mag/arcsec^2, μr~27 − 30 mag/arcsec^2, in the g and r bands, respectively.
Shallower data, with 1hr of integration time, are acquired in the i band during the bright time, which allows us to reach azimuthally averaged surface brightness of μg~25 mag/arcsec^2.
The observing strategy for Hα observations aims to detect Hα emission with a surface brightness of Σ(Hα) = 5 x 10-17 ergs/s/cm^2/arcsec^2. This level of depth guarantees the detection of Hα emission both in the inner star-forming regions of galaxies and possibly diffuse gas emission (e.g. Boselli et al. 2018, Kleiner et al. 2021).
Since all targets have a major axis diameter D $\leq$ 3 arcmin, the sky background can be estimated directly on the science frame, by using a polynomial surface fit over the entire frame (see Iodice et al. 2022).

Summary of the total integration time for each filter

g band: 2.5 hrs; FLI<0.3

r band: 2.5 hrs; FLI<0.5

i band: 1.0 hrs; FLI<0.9

Hα (NB_659): 1.0 hrs; FLI<0.9

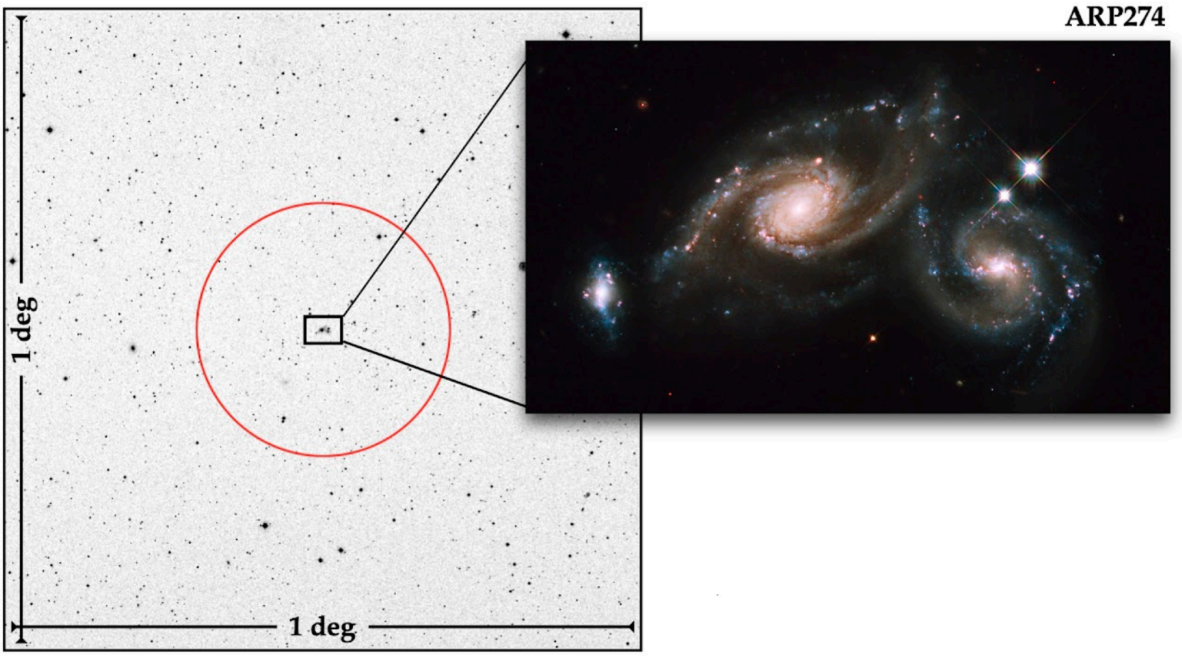

Figure 3: OmegaCam field of view (left panel) around the ARP274 galaxy (right panel), one of the target of this collection. The red circle marks the radius 10 times the optical diameter of the target.

Since the selected targets, listed in Table 1, span almost the whole range in RA, and the constraints set up cover all possible cases, i.e. dark time for the g band, grey time for the r band, and bright time for the i and Hα filters, this project is a filler program for VST.

Release Content

Arp nr. (1)	Object Name (2)	Mag [mag] (3)	Size [arcmin] (4)	Type (5)	RA [h m s] (6)	Dec [d m] (7)
RIGHT ASCENSION HOUR 0						
51	PGC 475	15.0	0.8' X 0.6'		00h06m16s	-13d26m
144	NGC 7828	14.4	0.9' X 0.5'	Ring A	00h06m27s	-13d24m
146	ARP 146		0.7' X 0.6'	Ring A	00h06m44s	-06d38m
246	NGC 7837	14.4	0.4' X 0.2'		00h06m51s	+08d21m
256	MCG-02-01-051	14.8	1.1' X 0.6'	SB(S)c pec	00h18m50s	-10d22m
35	PGC 001431	15.5	0.3' X 0.1'	Spiral	00h22m21s	-01d20m
201	MCG+00-02-018	16.0	0.4' X 0.2'		00h23m37s	-00d30m
100	IC 0018	15.0	1.5' X 0.8'	Sb	00h28m38s	-11d34m
127	NGC 0191	12.5	1.5' X 1.2'	SAB(rs)c:pec	00h38m59s	-09d00m
231	IC 1575	14.5	0.8' X 0.7'		00h43m33s	-04d07m
230	IC 0051	13.0	1.4' X 1.2'	SO pec?	00h46m24s	-13d26m
140	NGC 0274	13.0	1.5'	SAB(r:)0^0^ p	00h51m01s	-07d03m
251	VV 674	15.5	0.9' X 0.4'	Triple	00h53m46s	-13d51m
121	MCG-01-03-052	14.5	0.9' X 0.7'	Disrupted	00h59m23s	-04d48m
RIGHT ASCENSION HOUR 1						
59	NGC 0341A /B	14.5	1.1'	SAB(r)bc II	01h00m45s	-09d11m
236	IC 1623A/B	14.3	0.5' X 0.4'	S pec	01h07m47s	-17d30m
164	NGC 0455	12.6	2.0' X 1.2'	S?	01h15m57s	+05d10m
227	NGC 0470	11.9	2.8' X 1.8'	SA(r)b pec II	01h19m45s	+03d24m
227	NGC 0474	11.5	7.1' X 6.3'	(R')SAB0^0 pec	01h20m06s	+03d25m
67	UGC 00892	14.0	1.6' X 1.5'	SB(r)ab	01h21m16s	-00d32m
8	NGC 0497	13.0	2.1' X 0.9'	SB(r)b I-II	01h22m23s	-00d52m
157	NGC 0520	11.5	4.5' X 1.8'	S pec, Pair	01h24m35s	+03d47m
133	NGC 0541	12.1	1.8' X 1.8'	E0 or S0-	01h25m44s	-01d22m
308	NGC 0545/547	12.2	2.4' X 1.6'	E+3	01h25m59s	-01d20m

306	UGC 01102 group		1.3' X 1.1'	SBm	01h32m29s	+04d35m
4	MCG-02-05-050+ A	13.7	2.8' X 2.4'	IAB(rs)m	01h48m25s	-12d22m
228	IC 0162	13.7	1.6'	S0 -conc rings	01h48m53s	+10d31m
75	NGC 0702	11.9	1.6' X 1.2'	SAB(s)b: pec	01h51m18s	-04d03m
126	MCG+00-06-009 /010	14.5	1.2' X 0.7'		01h58m05s	+03d06m
RIGHT ASCENSION HOUR 2						
318	NGC 0833/35/38/39	12.7	1.5' X 0.7'	SAB(rs)c	02h09m20s	-10d07m
10	UGC 01775	13.8	1.5' X 1.5'	S?	02h18m26s	+05d39m
54	PGC 9107/MCG-01-07-007	17.1	0.5' X 0.3'		02h23m59s	-04d41m
309	NGC 0943/42	11.4	3.4'	S0^0: pec	02h29m09s	-10d49m
333	NGC 1024	12.1	3.9' X 1.4'	(R')SA(r)ab	02h39m12s	+10d50m
37	Messier 77	8.9	7.1' X 6.1'	(R)SAB(rs)ab	02h42m40s	-00d00m
77	NGC 1097/A	13.6	0.8' X 0.5'	E5 pec	02h46m09s	-30d13m
131	MCG-03-08-025 /26	14.5	1.0' X 0.7'		02h47m19s	-14d48m
118	NGC 1143/44	13.2	0.9' X 0.8'	Ring A	02h55m09s	-00d10m
RIGHT ASCENSION HOUR 3						
179	NPM1G -04.0134	16.6			03h01m40s	-04d40m
108	ESO 547-G002/03	15.0	0.6' X 0.4'	S0:	03h03m05s	-22d13m
332	MAC0307-2253 group		0.6' X 0.3'		03h07m59s	-22d53m
332	NGC 1229	13.9	1.4' X 0.9'	SB(s)ab: pec	03h08m11s	-22d57m
332	NGC 1228	13.2	1.5' X 0.9'	(R')SB(rs)0	03h08m11s	-22d55m
332	MAC0308-2253		0.5' X 0.2'		03h08m12s	-22d54m
332	NGC 1230	15.4	0.6' X 0.2'	SB0? p	03h08m16s	-22d59m
332	MAC0308-2300		0.3' X 0.2'		03h08m25s	-23d00m
332	MAC0308-2301		0.3'		03h08m26s	-23d01m
332	MCG-04-08-029	16.8	0.6' X 0.3'	S	03h08m26s	-23d02m
332	IC 1892	13.2	2.0' X 1.1'	SB(s)d pec	03h08m27s	-23d03m
41	NGC 1232 / A	10.1	7.5' X 6.5'	SAB(rs)c I-II	03h09m45s	-20d34m
304	NGC 1241	12.0	2.8' X 1.7'	SAB(rs)bc II	03h11m14s	-08d55m

147	IC 0298	15.0	0.7' X 0.5'	Ring A+B	03h11m18s	+01d18m
304	NGC 1242	13.7	1.2' X 0.7'	SB:(s:)cd III	03h11m19s	-08d54m
279	NGC 1253 / A	11.7	5.3' X 2.3'	SAB(s)cd	03h14m09s	-02d49m
39	NGC 1347	13.0	1.6' X 1.3'	SB(s)c: pec	03h29m42s	-22d16m
219	UGC 02812	14.9	0.9' X 0.8'	SB pec	03h39m51s	-02d06m
RIGHT ASCENSION HOUR 4-6						
20	UGC 03014	14.4	1.2' X 0.7'	SB?	04h19m53s	+02d05m
186	NGC 1614	13.6	1.3' X 1.2'	SB(s)c pec	04h33m59s	-08d34m
61	UGC 03104	15.1	1.0' X 0.5'	Sa	04h36m42s	-02d17m
180	MCG-01-13-034	14.8	1.1' X 0.5'	S	04h53m22s	-04d48m
259	Hickson 31	17.9	0.2' X 0.1'	S?	05h01m36s	-04d15m
187	MCG-02-13-040A	15.0	0.9' X 0.4'		05h04m53s	-10d14m
52	CGCG 421-027	15.6			05h19m44s	+03d43m
327	NGC 1875	13.6	1.6' X 0.5'	E2	05h21m45s	+06d41m
327	Hickson 34	18.4	0.2' X 0.1'	S0	05h21m47s	+06d41m
123	NGC 1888 /89	12.0	3.0' X 0.8'	Sb: pec sp	05h22m32s	-11d29m
RIGHT ASCENSION HOUR 8						
7	MCG-03-23-009	14.5	1.3' X 1.0'	SB(rs) bc:	08h50m17s	-16d34m
257	MCG+00-23-006/ 5	17.0	0.6' X 0.3'	S	08h51m37s	-02d21m
RIGHT ASCENSION HOUR 9						
275	NGC 2881	14.1			09h25m54s	-12d00m
237	MCG+02-24-013/ 14	15.3	1.1' X 0.5'	SBd	09h27m43s	+12d17m
232	NGC 2911	11.5	4.1' X 3.2'	SA(s)0: pec	09h33m46s	+10d09m
137	NGC 2914	13.2	1.0' X 0.7'	SB(s)ab	09h34m02s	+10d06m
221	MCG-02-25-006	14.0	1.3' X 1.1'		09h36m27s	-11d19m
142	UGC 05130 group (+ NGC2936 & NGC2937)	14.4	0.7' X 0.2'	E+SYS	09h37m43s	+02d46m
321	MCG-01-25-009 group	13.8	1.1' X 0.3'	Sbc	09h38m53s	-04d51m
253	UGCA 173 /175	16.1	1.3' X 0.2'	SB(s)dm?	09h43m24s	-05d16m
252	ESO 566-IG007 /8	15.3	0.8' X 0.5'	SBb pec?	09h44m58s	-19d43m
245	NGC 2992 /93	12.2	3.6' X 1.1'	S0 pec sp	09h45m42s	-14d19m
303	IC 0563 /64	14.7	0.9' X 0.5'	SB(r)ab: pec	09h46m20s	+03d02m

255	UGC 05304	14.3	1.1' X 0.9'	Pair	09h53m08s	+07d52m
292	IC 0575	13.2	1.7' X 1.2'	Sa pec sp	09h54m33s	-06d51m
RIGHT ASCENSION HOUR 10						
338	Arp 338		Pair		10h10m59s	-07d54m
44	UGC 05641 & IC609		0.3' X 0.3'		10h25m32s	-02d13m
53	NGC 3290	14.4	1.0' X 0.5'	SA(rs:)c: pec	10h35m17s	-17d16m
RIGHT ASCENSION HOUR 11						
335	NGC 3509	12.7	2.1' X 1.0'	SA(s)bc pec	11h04m23s	+04d49m
132	CGCG 011-053	15.5	0.4' X 0.3'	Pair	11h19m21s	-03d05m
5	NGC 3664	12.8	2.1' X 1.9'	SB(s)m pec	11h24m24s	+03d19m
161	UGC 06665	14.7	0.4' X 0.4'	Sb pec:	11h42m12s	+00d20m
248	MCG-01-30-32	14.5	1.2' X 0.6'	SAB(rs)b? pec	11h46m34s	-03d51m
248	MCG-01-30-33	14.1	1.8' X 0.7'	SB(s)b: pec	11h46m44s	-03d50m
248	MCG-01-30-34	15.0	1.0' X 0.7'	SB(s)c pec	11h46m49s	-03d49m
289	NGC 3981	11.0	5.3' X 2.3'	SA(rs)c pec	11h56m07s	-19d53m
22	ESO 572-G036	14.9	0.9' X 0.6'	IB(s)m	11h59m29s	-19d19m
22	NGC 4027	11.2	3.2' X 2.4'	SB(s)dm	11h59m30s	-19d15m
RIGHT ASCENSION HOUR 12						
244	NGC 4038	10.7	5.3' X 3.1'	SB?(s:)m pec	12h01m52s	-18d51m
244	NGC 4039	10.3	3.1' X 1.6'	IB:(s)m pec	12h01m53s	-18d53m
134	Messier 49	8.4	10.3' X 8.4'	E2	12h29m46s	+07d59m
277	NGC 4809	13.7	1.8' X 0.9'	Im pec	12h54m50s	+02d39m
277	NGC 4810	13.0	1.9' X 0.8'	Im pec	12h54m51s	+02d38m
RIGHT ASCENSION HOUR 13						
176	NGC 4933A	11.7	1.0' X 0.8'	S0 pec	13h03m54s	-11d30m
176	NGC 4933B	12.7	1.8' X 1.1'	E/S0 pec	13h03m56s	-11d29m
176	NGC 4933C	17.5	0.5' X 0.5'	Im: pec	13h03m58s	-11d30m
153	NGC 5128	6.8	25.9' X 20.1'	S0 pec	13h25m27s	-43d01m
326	MAC1337+0628		0.2'		13h37m11s	+06d28m
326	UGC 08610	15.4	1.2' X 0.4'	Sa	13h37m20s	+06d29m
326	MAC1337+0632		0.4' X 0.2'		13h37m21s	+06d33m
326	UGC 08613	15.0	1.4' X 0.6'	SB	13h37m24s	+06d26m
326	MCG+01-35-019	15.3	0.6' X 0.4'	S	13h37m25s	+06d31m

326	UGC 08613(a)	16	0.5' X 0.2'	E?	13h37m28s	+06d25m
33	UGC 08613	15.0	1.4' X 0.6'	SB	13h37m24s	+06d26m
33	UGC 08613(a)	16	0.5' X 0.2'	E?	13h37m28s	+06d25m
240	NGC 5257	12.9	1.8' X 0.9'	Sb? pec	13h39m53s	+00d50m
240	NGC 5258	12.9	1.7' X 1.1'	Sb? pec	13h39m57s	+00d49m
RIGHT ASCENSION HOUR 14						
271	NGC 5426	12.2	3.0' X 1.6'	SAB(rs)bc pec	14h03m25s	-06d04m
271	NGC 5427	11.4	2.8' X 2.4'	SA(s)c pec II	14h03m25s	-06d01m
286	NGC 5560	12.4	3.7' X 0.7'	SB(s)b pec	14h20m04s	+03d59m
286	NGC 5566	10.5	6.6' X 2.2'	SB(r)ab	14h20m20s	+03d55m
286	NGC 5569	13.2	1.7' X 1.5'	SAB(rs)cd	14h20m32s	+03d58m
49	NGC 5665	12.0	1.9' X 1.4'	SAB(rs)c pec?	14h32m25s	+08d04m
274	NGC 5679	13.0	1.1' X 0.6'	Sb	14h35m05s	+05d20m
274	NGC 5679A	13.5	1.2' X 0.7'	Sb	14h35m08s	+05d21m
274	NGC 5679C	15.0	0.2' X 0.1'		14h35m08s	+05d21m
171	IC 1042	14.9	1.1'	S0	14h40m37s	+03d27m
171	NGC 5718	12.9	1.5' X 1.1'	S0-:	14h40m43s	+03d27m
261	MCG-02-38-016	13.4	2.5' X 1.4'	IB(s)m pec	14h49m30s	-10d10m
261	MCG-02-38-017	14.5	2.5' X 1.4'	IB(s)m pec	14h49m32s	-10d09m
261	PGC 52943	14.9	0.8' X 0.7'		14h49m35s	-10d05m
173	MCG+02-38-019	15.6	1.0' X 0.2'	S?	14h51m26s	+09d19m
173	MCG+02-38-020	15.0	0.6' X 0.4'	S0:	14h51m27s	+09d19m
RIGHT ASCENSION HOUR 15						
254	NGC 5917	14.5	1.5' X 0.9'	Sb pec?	15h21m32s	-07d22m
RIGHT ASCENSION HOUR 22						
325	MAC2206-2105		0.3' X 0.1'		22h06m20s	-21d05m
325	MCG-04-52-014	18.1	0.4' X 0.4'	S0	22h06m21s	-21d04m
325	MAC2206-2104		0.3' X 0.2'		22h06m22s	-21d04m
325	MCG-04-52-014	17.9	0.4' X 0.3'		22h06m22s	-21d05m
325	MCG-04-52-014	16.0	0.3' X 0.3'		22h06m23s	-21d05m
226	NGC 7252	11.4	2.0' X 1.6'	SAB0^0? pec	22h20m44s	-24d40m
93	NGC 7284	11.9	2.1' X 1.5'	SB(s)0^0 pec	22h28m36s	-24d50m
93	NGC 7285	11.9	2.4' X 1.4'	SB(rs)a pec	22h28m38s	-24d50m

14	NGC 7314	10.9	4.6' X 2.1'	SAB(rs)c: II	22h35m45s	-26d03m
3	MCG-01-57-016	13.4	2.5' X 2.1'	SA(s)m	22h36m34s	-02d54m
15	NGC 7393	12.6	2.0' X 0.9'	SAB?(r:)b?	22h51m39s	-05d33m
110	MCG-03-58-011	15.9	0.7' X 0.6'	S	22h54m08s	-15d14m
314	MCG-01-58-009	13.7	1.1' X 0.9'	(R')SA(s)bc:	22h58m01s	-03d46m
314	MCG-01-58-010	13.8	1.3' X 1.1'	SB(rs)cd: pec	22h58m07s	-03d47m
314	MCG-01-58-011	16.0	1.1' X 0.9'	(R')SB(s)dm p	22h58m11s	-03d48m
RIGHT ASCENSION HOUR 23						
298	NGC 7469	12.3	1.5' X 1.1'	(R')SAB(rs)a	23h03m15s	+08d52m
298	IC 5283	13.8	0.8' X 0.4'	SA(r)cd pec?	23h03m18s	+08d53m
223	NGC 7585	11.4	2.3' X 2.0'	SA?0^0 pec	23h18m02s	-04d38m
92	NGC 7603	13.2	1.6' X 1.0'	SA(rs)0+: pec	23h18m56s	+00d14m
150	MCG+01-59-046	17.0	0.8' X 0.1'	S	23h19m28s	+09d30m
150	NGC 7609	14.9	0.8' X 0.5'	E3	23h19m30s	+09d30m
150	Hickson 96C	16.2	0.9' X 0.4'	Sm	23h19m31s	+09d30m
150	MCG+01-59-048	16.0	0.7' X 0.2'	Scd	23h19m34s	+09d30m
182	NGC 7674	13.9	1.0' X 1.0'	SA(r)bc pec	23h27m57s	+08d47m
182	MCG+01-59-081	15.4	0.5' X 0.3'	Sa	23h27m59s	+08d47m
182	PGC 071507	17.1	0.4' X 0.2'	Im	23h28m00s	+08d46m
182	NGC 7675	15.0	0.6' X 0.4'	E2	23h28m06s	+08d46m
216	NGC 7679	12.9	1.4' X 0.9'	(R':)Sc? pec	23h28m46s	+03d30m
216	NGC 7682	13.2	1.2' X 1.1'	SB(r)a: pec	23h29m03s	+03d32m
284	NGC 7714	12.5	1.9' X 1.4'	SB:(s)b? pec	23h36m14s	+02d09m
284	NGC 7715	14.2	2.6' X 0.5'	Sa? pec sp	23h36m22s	+02d09m
222	NGC 7727	10.6	4.7' X 3.6'	SAB:(s?)0/a p	23h39m54s	-12d17m
295	MCG-01-60-021	14.5	1.9' X 0.3'	Sc	23h41m47s	-03d40m
295	ARP 295	14.6	0.9' X 0.5'?	Sb pec	23h42m04s	-03d35m
68	NGC 7757	12.7	2.5' X 1.8'	SAB(rs)c	23h48m45s	+04d10m
323	NGC 7783	14.0	1.1' X 0.5'	S0^0:sp	23h54m10s	+00d23m
323	MCG+00-60-060	16.9	0.3' X 0.2'	Sc	23h54m11s	+00d24m
323	MCG+00-60-059	15.0	0.5' X 0.4'	S0	23h54m12s	+00d23m
323	MAC2354+0021		0.2' X 0.1'		23h54m13s	+00d21m
323	PGC 072810	16.3	0.3' X 0.2'	E	23h54m14s	+00d21m

Table 1. Target list of this collection. In column 1 and 2 are given the Arp number and the target name. In columns 3-7 are listed the magnitude (either b or V), size in arcminutes, morphological type and Right Ascension and Declination.

Release Notes

Data Reduction and Calibration

Data belonging to this release have been reduced using the Astronomical Wide-field Imaging System for Europe (Astro-WISE) pipeline (McFarland et al. 2013), also used for the KIDS survey. Below an overview of the pipeline.

Astro-WISE

The data released in this collection has been reduced by using the Astronomical Wide-field Imaging System for Europe (Astro-WISE) pipeline (McFarland et al. 2013), also used for the KIDS survey. The instrumental corrections applied for each frame include overscan correction, removal of bias, flat-fielding, illumination correction, masking of the bad pixels, and subtraction of the background.

- **De-biasing and overscan correction**. The data is overscan corrected by subtracting from each pixel row the row-wise median values, read from the CCD overscan areas. The fine structure of the bias is then subtracted using a master bias frame stacked from ten overscan corrected bias frames.
- **Flat-fielding.** Flatfielding is done after bias correction using a master flat-field which is combined from twilight flatfields and dome flatfields. Before combining the different flat-fields, the high spatial frequencies are filtered out from the twilight flat-fields, and the low frequency spatial Fourier frequencies from the dome flat-fields.
- **Weight maps.** During the instrumental reduction, weight maps are also created for each individual frame. Weight maps carry information about the defects or contaminated pixels in the images and also the expected noise associated with each pixel. The hot and cold pixels are detected from the bias and flatfield images, respectively. These pixels are then set to zero in the weight maps. The flatfielded and debiased images are also searched for satellite tracks and cosmic rays, and the values of the pixels in the weight maps corresponding to the contaminated pixels in the science images, are then set to zero.
- **Illumination correction.** Systematic photometric residual patterns still remain after flat-fielding, which are corrected by applying an illumination correction to the data. The correction models are made by mapping the photometric residuals across the OmegaCAM's CCD array using a set of dithered observations of Landolt's Selected Area (SA) standard star fields (A.U. Landolt, 1992, AJ, 104, 340), and fitting a linear model to the residuals. The images were multiplied with this illumination correction. The illumination correction is applied after the background removal to avoid producing artificial patterns in the background of images.
- **De-fringing.** De-fringing is only needed for i-band. Analysis of nightly fringe frames showed that the pattern is constant in time. For each science exposure this fringe image is scaled (after background subtraction of the science exposure and fringe frame) and then subtracted to minimize residual fringes.
- **Astrometric calibration.** The first-order astrometric calibration was done by first matching the pixel coordinates to RA and Dec using the World Coordinate System (WCS) information from the fits header. Point source coordinates were then extracted using SExtractor and associated with the 2 Micron All Sky Survey Point Source Catalog (2MASS PSC, Skrutskie et al. 2006). The transformation was then extended by a second-order two-dimensional polynomial across the focal plane. SCAMP (Bertin 2006) was used for this purpose. The polynomial was fit iteratively five times, each time clipping the 2σ-outliers. The astrometric solution gives typically rms errors of 0.3 arcsec (compared to 2MASS PSC) for a single exposure, and 0.1 arcsec for the stacked final mosaic.

- **Photometric calibration.** The absolute photometric calibration was performed by observing standard star fields each night and comparing their OmegaCAM magnitudes with the Sloan Digital Sky Survey Data Release 11 (SDSS DR11, Alam et al. 2015) catalog values. The OmegaCAM point source magnitudes were first corrected for the atmospheric extinction by subtracting a term kX, where X is airmass and k is the atmospheric extinction coefficient with the values of 0.182, 0.102 and 0.046 for g′, r′ and i′, respectively. The zero-point for a given CCD is the difference between the object's corrected magnitude measured from a standard star field exposure and the catalog value. The zero-point for each CCD was kept constant for the whole night, only correcting for the varying airmass.
- **Background subtraction.** There are different options to subtract the sky background in Astro-WISE, that are:
  0: Leave background subtraction to SWarp
  1: Create a background image outside SWarp, which gives better results than SWarp
  2: Subtract a constant as background, which is determined by iteratively clipping around the median pixel value
  When option 1 is chosen for the BACKGROUND_SUBTRACTION_TYPE, a background image is created. The process consists of these steps:
  1. Determine all pixels which are part of sources. This is done by running SExtractor on the image and using the "segmentation" check image.
  2. Exclude those pixels and calculate the median of the other pixels.
  3. Replace the pixels attributed to sources with the median calculated in the previous step.
  4. Run SExtractor to obtain the "background" check image. This is the background image that will be subtracted.
- **Regridding and coadding.** After the astrometric and photometric calibrations, the images were sampled to 0.20 arcsec pixel size and combined using the SWarp software (Bertin 2010). Before combining the images, cosmic rays and bad pixels were removed using the weight maps.

Data Quality

The limiting magnitudes within the field, for each target in the different photometric bands are:
- Depth_g [mag] ~ 26
- Depth_r [mag] ~ 25.5
- Depth_i [mag] ~ 24
- Depth_Hα (NB_659) [mag] ~ 23

while the average FWHM ranges between 0.4 and 0.8.
Same information is also reported in the image header. The limiting magnitude is the surface brightness of a point source corresponding at 5σ of the background noise in the image. The RMS error of the astrometric solution is ~0.3 arcsec.

Data Format

Files Types

The files are in FITS format, with the relevant information in the header. They have been compressed using NASA's HEASARC's fpack routine (https://heasarc.gsfc.nasa.gov/fitsio/fpack/).
Each science frame is accompanied by a weight frame. Files are named based on the field covered and the filter used for observations following the format:

<TargetName>_<FilterName>_sci.fits.fz for science images and
<TargetName>_<FilterName>_wei.fits.fz for weight maps.

Acknowledgements

According to the Data Access Policy for ESO data held in the ESO Science Archive Facility, all users are required to acknowledge the source of the data with appropriate citation in their publications.

Since processed data downloaded from the ESO Archive are assigned Digital Object Identifiers (DOIs), the following statement must be included in all publications making use of them:

- *Based on data obtained from the ESO Science Archive Facility with DOI: https://doi.eso.org/xxxx/archive/xxx*
- *Based on data collected with the INAF VST telescope at the ESO Paranal Observatory*

Publications making use of data which have been assigned an archive request number (of the form XXXXXX) must include the following statement in a footnote or in the acknowledgement:

- *Based on data obtained from the ESO Science Archive Facility under request number <request_number>.*

Science data products from the ESO archive may be distributed by third parties, and disseminated via other services, according to the terms of the Creative Commons Attribution 4.0 International license. Credit to the ESO provenance of the data must be acknowledged, and the file headers preserved.